Environmental Science
Processes & Impacts

Accepted Manuscript

ROYAL SOCIETY OF CHEMISTRY

rsc.li/process-impacts

Table of Content

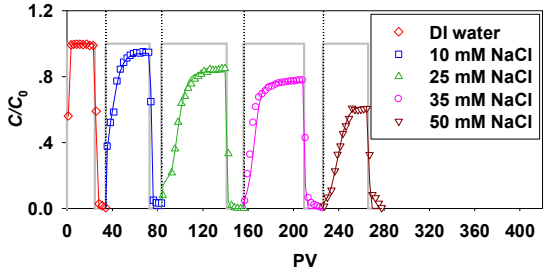

Graphene oxide nanoparticles can be highly mobile in saturated soils, even at high ionic strength.

Environmental Impact Statement

Graphene oxide (GO) is an important engineered carbon nanomaterial with many promising applications. However, the increasing production and use of GO will increase the likelihood of its environmental release. In aqueous environment GO can form colloidal GO nanoparticles (GONPs). Because GO has strong adsorption affinities for a range of environmental contaminants, GONPs may significantly enhance the transport and risks of contaminants by serving as a contaminant carrier. This study demonstrates that GONPs can be highly mobile in saturated sandy soil under a range of solution chemistry conditions and flow velocities. The high mobility of GONPs may have important implications for their environmental fate and effects.

Transport of Graphene Oxide Nanoparticles in Saturated Sandy Soil

Zhichong Qi,[a] Lunliang Zhang,[a,b] and Wei Chen[*,a]

[a] College of Environmental Science and Engineering/Ministry of Education Key Laboratory of Pollution Processes and Environmental Criteria/Tianjin Key Laboratory of Environmental Remediation and Pollution Control, Nankai University, Wei Jin Road 94, Tianjin 300071, China

[b] Tianjin Environmental Protection Bureau, Fu Kang Road 17, Tianjin, 300191, China

*Corresponding author

E-mail address: chenwei@nankai.edu.cn

Phone/fax number: 86-22-66229516

Abstract

We examined the transport properties of graphene oxide nanoparticles (GONPs) in saturated sandy soil, under different solution chemistry conditions and flow velocities. GONPs exhibited high mobility in soil, even at 50 mM NaCl. While at relatively high ionic strength GONPs were less mobile in soil than in quartz sand, the differences were not significant. At a concentration of 0.5 mM, Ca^{2+} significantly inhibited the transport of GONPs in soil, but only slightly inhibited the transport in quartz sand. This was because by complexing with the surface O-functionalities of both GONPs and soil components, Ca^{2+} could enhance the aggregation of GONPs and bridge GONPs and soil grains. Increasing pH from 4 to 9 only slightly enhanced the transport of GONPs in soil, probably because the mobility of GONPs was already high at low pH. The presence of 10 mg/L Suwannee River humic acid significantly enhanced the transport of GONPs in quartz sand at 35 mM, but only had a small effect for the transport in soil. This was possibly linked to the much smaller grain sizes and much more heterogeneous nature of the soil. Flow velocity had marked effects on the transport in soil, but essentially no effects on the transport in quartz sand. A two-site transport model incorporating both the blocking-affected attachment process and straining effects can effectively model the transport of GONPs. The high mobility of GONPs may have important implications for their environmental fate and effects.

1 Introduction

Graphene and graphene-based nanomaterials are a new class of carbonaceous nanomaterials that have shown great promises in a number of applications, such as energy-related materials, sensors, biomedical applications, to mention a few.[1,2] Mass production and manipulation of graphene and graphene-based nanomaterials are commonly achieved by chemical modification of graphene oxide (GO). Additionally, GO itself is an excellent candidate for many applications (e.g., energy, biomedical, etc.).[3] As with other engineered nanomaterials, the rapidly increasing production and use of GO will likely cause its release into the environment, with unknown implications. Recently, the environmental fate, transport, and human-health risks of GO have received much attention.[4-8]

An important property of GO is that it contains large amounts of surface O-functionalities, such as carboxyl, carbonyl, hydroxyl, and phenol.[3] These different surface O-functional groups cover a range of acid dissociation coefficients (K_a).[9] Thus, GO can possess negative surface charges under relatively wide ranges of environmental conditions and can disperse easily in aqueous solution,[10,11] without having to undergo solvent exchange or sonication, and without requiring the addition of stabilizing reagents. While this relatively hydrophilic nature gives GO greater compatibilities in many areas of applications, it probably also makes it more mobile than many other carbon nanomaterials, even the surface oxidized ones.

To date, only a few literature papers are available on the transport of GO nanoparticles (GONPs) in porous media,[5-7] and all the porous materials tested were purified quartz sands (pre-treated to remove metal oxides and natural organic matter). It has been observed that GONPs exhibit high mobility in quartz sand, the interactions between GONPs and quartz sand largely follow the Derjaguin–Landau–Verwey–Overbeek (DLVO) theory, and ionic strength can

significantly influence the transport of GONPs by affecting both the surface charges and particle sizes of GONPs.[7] Thus far, the transport properties of GONPs in saturated soils have not been reported. Compared with purified quartz sands, soil grains are much more heterogeneous both physically (e.g., size, shape, roughness) and chemically (e.g., different soil components possess different surface properties). For example, clay minerals, metal oxides, and soil organic matter of soil grains can interact with nanoparticles via very different mechanisms than does quartz sand. Thus, the transport properties of GONPs in soils cannot be extrapolated with the transport properties in purified quartz sands, and systematical studies are much needed.

The primary objective of this study was to understand the transport properties of GONPs in saturated sandy soils under a variety of environmental conditions. A low-organic-carbon sandy soil was selected as a model porous medium, and a purified quartz sand was also included as a comparison medium. The transport data of GONPs under different solution chemistry conditions (i.e., ionic strength, monovalent/divalent cations, pH, SRHA) and flow velocities were examined. The mechanisms controlling the transport of GONPs in the sandy soil, as well as the differences between the transport properties in soil and in sand, were analyzed. A two-site transport model was applied to simulate the transport data.

2 Experimental

2.1 Materials

Graphene oxide (>99%) was obtained from Plan Nano Materials Tech Co. (Tianjin, China). The GO product contained 62.1% C (wt:wt), measured using an automatic elemental analyzer (Vario EL CUBE, Elementar Analysensysteme, Hanau, Germany). The surface C/O atomic ratio (2.2) was determined with X-ray photoelectron spectroscopy (MultiLab 2000, Thermo Electron

Corp., England). The existence of –C–O, –C=O, and –OH functional groups were confirmed with Fourier transform infrared transmission spectra (Bruker TENSOR 27 apparatus, Bruker Optics Inc., Germany). The Brunauer–Emmer–Teller surface area of the GO (207.1 m^2/g) was calculated using the adsorption data of N_2.

Lula soil, containing 45% sand, 36% silt, and 19% clay,[12] was collected from a ranch near Lula, OK, USA. The organic carbon content of the soil was 0.37%. The average grain size of the soil was 120 μm. Sigma sand, with an average grain diameter of 260 μm, was purchased from Sigma–Aldrich (St. Louis, MO, USA). The sand was cleaned to remove metal oxides and organic contaminants using the method of Mattison et al.[13]

Suwannee River humic acid (SRHA) was purchased from the International Humic Substance Society (St. Paul, MN, USA). SRHA was composed of 52.6% C (wt:wt), 4.3% H, 42.0% O, and 1.2% N. The distribution of functional groups was carboxylic (15%), aromatic (31%), aliphatic (29%), and carbonyl (6%). The concentrations of SRHA are expressed as mg SRHA per liter of solution in this paper.

2.2 Preparation and characterization of GONPs

The stock suspension of GONPs was prepared using the following procedures. First, approximately 30 mg GO powder was added to 300 ml deionized (DI) water in a glass beaker. The mixture was ultra-sonicated at 100 W (Vibra-Cell VCX800, Sonics & Material, Newtown, CT, USA) for 30 min. Afterward, the suspension was filtered with 0.45-μm membrane filters (Millipore Co., Billerica, MA, USA) to remove large aggregates. The concentration of GONPs in the stock suspension was verified by measuring the total organic carbon,[14] with a high sensitivity total organic carbon analyzer (Shimadzu Scientific Instruments, Columbia, MD, USA). The

obtained stock suspension was stored in dark at 4 ºC. Working suspensions of GONPs (i.e., the influents of the column experiments) were obtained by diluting the stock suspension in electrolyte solutions.

The ζ potential values of the GONP suspensions were determined by electrophoretic mobility, using a ZetaPALS (Brookhaven Instruments, Holtsville, NY, USA). Dispersion properties of the GONP suspensions were determined with a JEM-2100 transmission electron microscope (TEM) (JEOL, Tokyo, Japan), and the samples were prepared by air-drying a drop of suspension onto a copper TEM grid (Electron Microscopy Sciences, Hatfield, PA, USA). Atomic force microscope (AFM) images were obtained with a J scanner of a Veeco Multimode Nanoscope VIII (Santa Barbara, CA, USA); the detailed sample preparation methods are given in Supplementary Information (SI).

2.3 Column transport experiments

Lula soil or Sigma sand was dry-packed into Omnifit borosilicate glass columns (10 cm × 0.66 cm, Bio-Chem Valve Inc., Boonton, NJ, USA) with 10-μm stainless-steel screens (Valco Instruments Inc., Houston, TX, USA) on both ends. The packed columns were equilibrated by sequentially flushing with 100 ml DI water at a flow rate of 3 ml/h followed by 180 ml background electrolyte solution. The porosity and dead volume were determined by inverse fitting the breakthrough curves (BTCs) of KBr (used as a conservative tracer).

The experimental protocols of the column experiments are given in Table 1. In a typical column experiment, the influent was pumped into the column with a syringe pump (KD Scientific, Holliston, MA, USA), followed by a GONP-free background electrolyte solution (until the concentration of GONPs in the effluent was below the detection limit); next, the same

GONP-containing influent (at a different flow velocity) or another GONP-containing influent (with a different background electrolyte) was pumped through the column. (Note that it is possible that a small amount of GONPs was retained in the column even after flushing with an electrolyte; however, the retained particles should have little effect on the deposition of GONPs during the subsequent experiments, because the mass of GONPs retained was generally negligible.) Column effluent samples were collected in 4-ml glass vials every 2–3 pore volumes (PV) to determine the concentrations of GONPs.

The concentrations of GONPs in the influent (C_0) and effluent (C) were determined by measuring the UV absorbance at 230 nm (with a UV-2401 UV/vis spectrophotometer, Shimadzu Scientific Instruments, Japan), based on a pre-established calibration curve of GO.[15] The detection limit of GO was 0.03 mg/L. In the presence of SRHA, the concentrations of GONPs were determined using the method of Chen et al.,[16] by obtaining the calibration curve of UV absorbance of GO (at 230 nm) as a function of GO concentration in the presence of 10 mg/L SRHA (SI Fig. S1).

2.4 Two-site transport model

A two-site transport model developed by Bradford et al.[17] was used to fit the BTCs of GONPs. The model divides the deposition sites into an attachment site and a straining site ("straining" was used as a collective term for wedging, referring to the retention of particles at two bounding surfaces, and bridging, referring to the situation that multiple particles collide and are retained in a pore constriction[18]):

$$\frac{\partial C}{\partial t}+\frac{\rho}{\theta}\frac{\partial S_1}{\partial t}+\frac{\rho}{\theta}\frac{\partial S_2}{\partial t}=D\frac{\partial^2 C}{\partial x^2}-v\frac{\partial C}{\partial x} \quad (1)$$

$$\frac{\rho}{\theta}\frac{\partial S_1}{\partial t} = K_{att}\psi_1 C \quad (2)$$

$$\frac{\rho}{\theta}\frac{\partial S_2}{\partial t} = K_{str}\psi_2 C \quad (3)$$

where ρ (g/cm^3) is the dry bulk density of the packed column; θ (-) is the porosity of the packed column; D (m^2/d) is the hydrodynamic dispersion coefficient; v (m/d) is the pore-water velocity; C (mg/L) is the concentration of GONPs in the aqueous phase at time t (h) and a distance x (cm); S_1 (mg/kg) and S_2 (mg/kg) are the concentrations of GONPs in the attachment site and the straining site, respectively; K_{att} (h^{-1}) and K_{str} (h^{-1}) are the attachment rate and straining rate, respectively; ψ_1 (-) and ψ_2 (-) are the blocking factor and straining factor.

The blocking factor ψ_1 can be expressed as:

$$\psi_1 = \frac{S_{max} - S_1}{S_{max}} \quad (4)$$

where S_{max} (mg/kg) is the maximum retention capacity of GONPs in the attachment site. The straining factor ψ_2 can be described as:

$$\psi_2 = \left(\frac{d_c + z}{d_c}\right)^{-\beta} \quad (5)$$

where d_c (cm) is mean grain diameter of the sand; z (cm) is the down gradient distance from the porous medium inlet; and β (-) is a fitting parameter that controls the shape of nanoparticle spatial distribution. A value of 0.432 was assigned for β.[17]

To obtain the D value of each column, the BTCs of KBr were fitted with the one-dimensional steady-state advection–dispersion equation using the CXTFIT code.[19] The BTCs of GONPs were fitted with Equations 1–5 using the HYDRUS-1D software[20] ,with K_{att}, S_{max}, and K_{str} as the fitting parameters.

In case clogging occurred in a column, Equation 5 was modified as:

$$\psi_2 = \max(1, S_2^{S'_{\max}}) \quad (6)$$

where a separate $s'_{\max}$ (mg/kg) was assumed for the site. In this case, K_{att}, S_{max}, K_{str}, and $s'_{\max}$ were used as the fitting parameters.

3 Results and Discussion

The transport properties of GONPs in Lula soil and Sigma sand under different solution chemistry conditions (i.e., ionic strength, monovalent/divalent cations, pH, SRHA) and flow velocities are shown in Fig. 1–6. The BTCs of GONPs were fitted with the two-site transport model (Equations 1–6). The fitted BTCs are shown in Fig. 1 and 3–6, and the fitted model parameters are summarized in SI Table S1. Under all the test experimental conditions the BTCs of GONPs can be sufficiently modeled.

3.1 Effects of ionic strength

The BTCs of GONPs in Lula soil at different ionic strength are shown in Fig. 1, and the BTCs in Sigma sand are also shown as the comparisons. It can be seen that transport of GONPs responded appreciably with the increase of ionic strength. Fig. 1a shows that when the influent contained no salt (i.e., GONPs in DI water), 100% breakthrough of GONPs from the soil column (as indicated by the C/C_0 value) was reached within 4 PV. With the increase of ionic strength from 0 to 50 mM NaCl, the maximum breakthrough (i.e., the maximum C/C_0 value) was reached more slowly and to gradually smaller values, indicating that more GONPs were retained in the column with the increase of ionic strength. The observed effects of ionic strength are in general consistent with the mechanisms governing the transport of negatively charged nanoparticles,

188 such as nC$_{60}$,[21,22] and are in line with the DLVO theory. According to the DLVO theory,
189 increasing ionic strength compresses double layer thickness and reduces double layer repulsion
190 between nanoparticles and grain surfaces.[23] Additionally, the secondary energy minimum
191 between particles and collector also increase with increasing ionic strength.[7] Similar observations
192 have been made for the transport of GONPs in quartz sand.[5,7]

193 Note that when the ionic strength of the influent was increased from 0 to 10 mM NaCl, the
194 breakthrough of GONPs from Lula soil was only slightly inhibited (Fig. 1a), only at 25 mM
195 NaCl and above was significant retention of GONPs observed. However, even at 50 mM NaCl,
196 the maximum C/C_0 value still reached approximately 60%. Furthermore, while at relatively high
197 ionic strength GONPs exhibited greater mobility in Sigma sand than in Lula soil, the differences
198 were not very significant, even though Lula soil contained considerable amounts of impurities
199 (compared with the pre-cleaned sand) that can be positively charged under the test conditions
200 and thus served as the favorable deposition sites of GONPs.[24] The high mobility of GONPs in
201 soil is attributable to the relatively strong negative surface charges of GONPs (SI Table S2) –
202 even at 50 mM NaCl GONPs still possessed negative surface charges, with a ζ potential value of
203 -14.6 mV. The pK_a values of the surface O-functional groups of GO cover a relatively wide
204 range, from 4.3 to 9.8,[9] which allows GONPs to possess negative surface charges within a
205 relatively wide range of solution chemistry conditions. This is a special characteristic that
206 distinguishes GONPs from other carbon nanoparticles. Additionally, the charge heterogeneity on
207 the grain surface of Lula soil can be masked by the presence of natural organic matter.[25-27]

208 In Fig. 2 the fitted values of K_{att}, S_{max}, and K_{str} are plotted against ionic strength. The
209 increases of K_{att} and S_{max} with ionic strength are consistent with the DLVO theory. Interestingly,
210 a more drastic increase of K_{str} was observed at 50 mM NaCl for both the soil and sand columns.

The increase in the K_{str} value was likely caused by the increase in particle size with increasing ionic strength – the TEM images and AFM height profiles (SI Fig. S2 and S3) clearly show that aggregation of GONPs at 50 mM was much more significant than at the lower ionic strength (consequently, the ratio of the particle diameter to soil grain diameter reached approximately 0.005). Fig. 2 also shows that the effects of increasing ionic strength on S_{max} and K_{str} are more significant for Lula soil than for Sigma sand. This can probably be attributed to the heterogeneous nature of Lula soil, compared with the pre-cleaned Sigma sand. First, because the compositions of natural soil are much more complex than quartz sand, soils may respond to the changes of ionic strength differently than pure sand.[21] Second, Lula soil is considerably finer in size and more heterogeneous in terms of particle size than Sigma sand. Accordingly, the significance of straining for the column packed with Lula soil (which expectedly had smaller pores and more tortuous pore structures) would be more sensitive to the increase of the sizes of GONPs.

3.2 Effects of divalent cations

The effects of divalent cations species (using Ca^{2+} as a model divalent cation) on the transport of GONPs are shown in Fig. 3. Compared with monovalent cation (i.e., Na^{+}) Ca^{2+} had much greater effects on the transport of GONPs in Lula soil. Fig. 3a shows that when the influent contained 1.5 mM NaCl, the C/C_0 value of GONPs rapidly reached nearly 100% after only 5 PV (the BTC essentially overlaps with the BTC of GONPs in DI water; see SI Fig. S4). After switching to the influent containing 0.5 mM $CaCl_2$ (with the same ionic strength as 1.5 mM NaCl) the maximum C/C_0 value only reached 36% and then gradually decrease to zero, after approximately 30 PV of influent was pumped through the column, indicating the clogging of the

column. A separate experiment was carried out by increasing the concentration of Ca^{2+} in the influent step-wise, from 0.1 to 0.3 to 0.5 mM (Fig. 3b). The results show that clogging of soil column only occurred at 0.5 mM. Thus, under the experimental conditions the critical Ca^{2+} concentration that would result in the clogging of soil column is likely between 0.3 to 0.5 mM. Interestingly, for Sigma sand a much smaller effect of Ca^{2+} was observed, in that switching the influent from GONPs in 1.5 mM NaCl to GONPs in 0.5 mM Ca^{2+} only resulted in slight decrease in the breakthrough of GONPs – the C/C_0 value decreased from 100% to 95% (Fig. 3c).

As shown in Table S2, the ζ potential of GONPs in 0.5 mM $CaCl_2$ (-14.0 mV) is similar to the ζ potential of GONPs in 50 mM NaCl. However, much more inhibited transport of GONPs was observed at 0.5 mM $CaCl_2$ than at 50 mM NaCl (-14.6 mV). Evidently, the effects of Ca^{2+} cannot be explained with the DLVO theory. The strong transport-inhibition effects of Ca^{2+} likely stemmed from the effects of Ca^{2+} on the aggregation of GONPs. As mentioned earlier, GO is rich in surface O-functionalities. Because Ca^{2+} can form complexes with some of the surface O-functional groups,[28] Ca^{2+} can serve as a bridging agent to bind GO flakes. Consequently, at a given ionic strength Ca^{2+} can result in much more significant aggregation of GONPs than monovalent ions. The AFM height profiles in Fig. S3 clearly show that the GONP aggregates formed in 0.5 mM Ca^{2+} were considerably larger than those formed in 50 mM NaCl. Another possible mechanism controlling the strong effect of Ca^{2+} on the transport of GONPs is that Ca^{2+} could also serve as a bridging agent by forming complexes with both GO flakes and surface functional groups of soil grains, and therefore, enhance the deposition of GONPs. This mechanism is consistent with the fact that Ca^{2+} had much more significant effects on the transport of GONPs in Lula soil than in Sigma sand, because the soil contains more complexation sites for Ca^{2+}, such as clay minerals and natural organic matter.[21,29]

3.3 Effects of pH

The effects of pH on the transport of GONPs are shown in Fig. 4. In general, within the test pH range (4 to 9) increasing pH resulted in enhanced transport of GONPs in Lula soil, but the effects were relatively small. Because pH had minimal effects on the ζ potential of GONPs (Table S2), the observed small transport-enhancement effects were largely linked to the effects of pH on soil grains. It has been proposed that the surface charges of both quartz and clay minerals become more negative with increasing pH.[30] More importantly, under unfavorable deposition conditions pH can affect transport of nanoparticles by masking the heterogeneities of grain surfaces (e.g., metal oxides)[31,32] – the surfaces of certain soil minerals (such as Al_2O_3 and Fe_2O_3) can be positively charged at acidic pH,[33] and increasing pH can eliminate and even reverse such positive surface sites.[34,35] However, this effect was likely negligible for Sigma sand, which was pre-cleaned to remove metal oxides. This is in line with the negligible effects of pH on the transport of GONPs in Sigma sand (Fig. 4b).

3.4 Effects of dissolved organic matter

The effects of dissolved organic matter on the transport of GONPs were tested at two different ionic strength, using SRHA as a model dissolved organic matter; the results are shown in Fig. 5. A striking observation was that at both ionic strength (i.e., 10 mM NaCl and 35 mM NaCl) the presence of 10 mg/L of SRHA in the influent only had a small effect on the transport of GONPs in Lula soil but a more significant effect on the transport in Sigma sand. At 10 mM NaCl the maximum C/C_0 value of the soil column increased from 96% (in the absence of SRHA) to 99% (in the presence of SRHA), and at 35 mM the maximum C/C_0 value increased from 63%

to 71%. However, at 35 mM NaCl the maximum C/C_0 value of the sand column increased from 81% (in the absence of SRHA) to nearly 100% (in the presence of SRHA). It has been proposed that under unfavorable deposition conditions humic acids can affect the transport of nanoparticles via two major mechanisms. First, adsorption of humic acids to nanoparticles and to the surfaces of soil/sand grains could enhance the steric and electrostatic repulsions between the nanoparticles and the packed materials, and thus, inhibiting the deposition of nanoparticles.[16,29,36-38] However, this effect could be less important for Lula soil than for quartz sand because natural soils already contain soil organic matter. Second, adsorption of humic acids to nanoparticles can affect particle size, and consequently affect the extent of deposition via straining. A possible explanation for the much weaker effects of SRHA on the transport of GONPs in Lula soil than in Sigma sand is that the SRHA-induced changes of particle sizes play a relatively minor role in the transport in soil columns than in sand columns: because soil grains are much smaller and much more heterogeneous than quartz sand, the pores in soil columns are likely smaller and more tortuous; therefore, reduction in particle size may not necessarily result in much enhanced transport (i.e., the extent of enhanced transport depends on whether the reduction in particle sizes is significant compared with the pore sizes of packed soil). Note that the TEM images (Fig. S2) and AFM height profiles (Fig. S3) show that even though SRHA significantly inhibited the stacking of GO flakes at high ionic strength, the areal dimensions of GONPs were not much affected. Thus, even for the SRHA-modified GONPs significant straining could still have been an important mechanism controlling the transport in Lula soil.

3.5 Effects of flow velocity

The effects of flow velocity on the transport of GONPs in Lula soil and Sigma sand are shown in Fig. 6. While flow velocity had marked effects on the transport in Lula soil, it had essentially no effects on the transport in Sigma sand. Interestingly, for the column packed with Lula soil the changes in the maximum C/C_0 value correlate well with the changes of flow velocity – the maximum C/C_0 value decreased from 98% (corresponding to a flow velocity of 10 m/d), to 91% (5 m/d), to 79% (1 m/d). The observed velocity effects are consistent with the literature reports.[39-41] For example, Li et al.[39] observed enhanced nC$_{60}$ retention at a pore-water velocity of 1 m/d than at 8 m/d. The strikingly different responses of transport properties to the changes of flow velocity between the column packed with Lula soil and that with Sigma sand seem to be consistent with the theory of flow stagnation zones. Johnson et al.[42] proposed that retention in flow stagnation zones is an important mechanism for colloid retention under unfavorable attachment conditions, and the volumes of flow stagnation zones decrease with increasing flow velocity. It is reasonable to assume that larger volumes of stagnation zones exist in the columns packed with more heterogeneous, rough-surfaced, and irregularly shaped materials (e.g., soil) than more homogeneous materials (e.g., quartz sand).

4 Conclusions

One characteristic that distinguishes GO from other forms of oxidized carbon nanomaterials (e.g., surface oxidized carbon nanotubes) is its high surface O-content. This allows GONPs to possess strong negative surface charges within a relatively wide range of solution chemistry conditions. The findings of this study indicate that GONPs can be quite mobile in the environment, which can potentially increase their environmental risks. The high mobility, in combination with the strong adsorption affinities of GONPs to a variety of environmental

contaminants,[43-46] also makes GONPs potentially superior carriers for environmental contaminants. In view of the increasing mass production and use of GO, these potential risks should be given full considerations, to fully understand the environmental implications of this new engineered nanomaterial and to ensure its beneficial use.

Acknowledgement

This project was supported by the Ministry of Science and Technology of China (Grant 2014CB932001), and the National Natural Science Foundation of China (Grants 21237002 and 21177063).

Supplementary Information

Electronic supplementary information (ESI) may be found in the online version of this article.

References

1 A. K. Geim and K. S. Novoselov, The rise of graphene, *Nat. Mater.*, 2007, **6,** 183–191.

2 S. Park and R. S. Ruoff, Chemical methods for the production of graphenes, *Nat. Nanotechnol.*, 2009, **4,** 217–224.

3 D. R. Dreyer, S. Park, C. W. Bielawski and R. S. Ruoff, The chemistry of graphene oxide, *Chem. Soc. Rev.*, 2010, **39,** 228–240.

4 I. Chowdhury, M. C. Duch, N. D. Mansukhani, M. C. Hersam and D. Bouchard, Colloidal properties and stability of graphene oxide nanomaterials in the aquatic environment, *Environ. Sci. Technol.*, 2013, **47,** 6288–6296.

5 L. Feriancikova and S. Xu, Deposition and remobilization of graphene oxide within saturated sand packs, *J. Hazard. Mater.*, 2012, **235,** 194–200.

6 L. Liu, B. Gao, L. Wu, V. L. Morales, L. Yang, Z. Zhou and H. Wang, Deposition and transport of graphene oxide in saturated and unsaturated porous media, *Chem. Eng. J.*, 2013, **229,** 444–449.

7 J. D. Lanphere, C. J. Luth and S. L. Walker, Effects of solution chemistry on the transport of graphene oxide in saturated porous media, *Environ. Sci. Technol.*, 2013, **47,** 4255–4261.

8 O. Akhavan and E. Ghaderi, Toxicity of graphene and graphene oxide nanowalls against bacteria. *ACS Nano*, 2010, **4,** 5731–5736.

9 B. Konkena and S. Vasudevan, Understanding aqueous dispersibility of graphene oxide and reduced graphene oxide through pK_a measurements, *J. Phys. Chem. Lett.*, 2012, **3,** 867−872.

10 Y. Si and E. T. Samulski, Synthesis of water soluble graphene, *Nano Lett.*, 2008, **8,** 1679–1682.

11 D. Li, M. B. Müller, S. Gilje, R. B. Kaner and G. G. Wallace, Processable aqueous dispersions of graphene nanosheets, *Nat. Nanotechnol.*, 2008, **3,** 101–105.

12 L. Zhang, L. Wang, P. Zhang, A. T. Kan, W. Chen, and M. B. Tomson. Facilitated transport of 2,2',5,5'-polychlorinated biphenyl and phenanthrene by fullerene nanoparticles through sandy soil columns, *Environ. Sci. Technol.*, 2011, **45,** 1341–1348.

13 N. T. Mattison, D. M. O'Carroll, R. Kerry Rowe and E. J. Petersen. Impact of porous media grain size on the transport of multi-walled carbon nanotubes, *Environ. Sci. Technol.*, 2011, **45,** 9765–9775.

14 X.W. Wang, H. W. Tian, Y. Yang, H. Wang, S. M. Wang, W. T. Zheng and Y. C. Liu, Reduced graphene oxide/CdS for efficiently photocatalystic degradation of methylene blue, *J. Alloys. Compd.*, 2012, **524,** 5–12.

15 G. Wang, B. Wang, J. Park, J. Yang, X. Shen and J. Yao, Synthesis of enhanced hydrophilic and hydrophobic graphene oxide nanosheets by a solvothermal method, *Carbon*, 2009*,* **47,** 68–72.

16 G. Chen, X. Liu and C. Su, Distinct effects of humic acid on transport and retention of TiO_2 rutile nanoparticles in saturated sand columns, *Environ. Sci. Technol.*, 2012, **46,** 7142–7150.

17 S. A. Bradford, J. Simunek, M. Bettahar, M. T. van Genuchten, and S. R. Yates, Modeling colloid attachment, straining, and exclusion in saturated porous media, *Environ. Sci. Technol.*, 2003, **37,** 2242–2250.

18 G. Gargiulo, S. A. Bradford, J. Simunek, P. Ustohal, H. Vereecken and E. Klumpp, Bacteria transport and deposition under unsaturated flow conditions: the role of water content and bacteria surface hydrophobicity, *Vadose Zone J.*, 2008, **7,** 406–419.

19 F. J. L. N. Toride and M. T. van Genuchten, *The CXTFIT Code for Estimating Transport Parameters from Laboratory or Field Tracer Experiments*; U.S. Salinity Laboratory: Riverside, CA, 1999.

20 J. Simunek, M. T. van Genuchten and M. Sejna, *The HYDRUS-1D Software Package for Simulating the One-Dimentional Movement of Water, Heat, and Multiple Solutes in Variably-Saturated Media: Version 3.0*, Department of Environmental Science, University of California Riverside: Riverside, CA, 2005.

21 L. Zhang, L. Hou, L. Wang, A. T. Kan, W. Chen and M. B. Tomson, Transport of fullerene nanoparticles (nC_{60}) in saturated sand and sandy soil: Controlling factors and modeling, *Environ. Sci. Technol.*, 2012, **46,** 7230–7238.

22 Y. Wang, Y. Li and K. D. Pennell, Influence of electrolyte species and concentration on the aggregation and transport of fullerene nanoparticles in quartz sands, *Environ. Toxicol. Chem.*, 2008, **27,** 1860–1867.

23 J. N. Ryan and M. Elimelech, Colloid mobilization and transport in groundwater. *Colloids Surf., A*, 1996, **107,** 1–56.

24 G. Cornelis, L. Pang, C. Doolette, J. K. Kirby and M. J. McLaughlin, Transport of silver nanoparticles in saturated columns of natural soils, *Sci. Total Environ.*, 2013, **463–464,** 120–130.

25 B. Pan and B. Xing, Applications and implications of manufactured nanoparticles in soils: A review. *Eur. J. Soil Sci.*, 2012, **63,** 437–456.

26 H. F. Lecoanet, J. Y. Bottero and M. R. Wiesner, Laboratory assessment of the mobility of nanomaterials in porous media. *Environ. Sci. Technol.*, 2004, **38,** 5164–5169.

27 Y. Liang, S. A. Bradford, J. Simunek, M. Heggen, H. Vereecken and E. Klumpp, Retention and remobilization of stabilized silver nanoparticles in an undisturbed loamy sand soil. *Environ. Sci. Technol.*, 2013, **47,** 12229–12237.

28 S. Park, K.S. Lee, G. Bozoklu, W. Cai, S. T. Nguyen and R. S. Ruoff, Graphene oxide papers modified by divalent ions—Enhancing mechanical properties via chemical cross-linking, *ACS Nano*, 2008, **2,** 572–578.

411 29 K. L. Chen and M. Elimelech, Interaction of Fullerene (C_{60}) nanoparticles with humic acid
412 and alginate coated silica surfaces: Measurements, mechanisms, and environmental
413 implications. *Environ. Sci. Technol.*, 2008, **42,** 7607–7614.
414 30 A. Kaya and Y. Yukselen, Zeta potential of clay minerals and quartz contaminated by heavy
415 metals, *Can. Geotech. J.*, 2005, **42,** 1280–1289 .
416 31 L. Song, P. R. Johnson and M. Elimelech, Kinetics of colloid deposition onto heterogeneously
417 charged surfaces in porous media. *Environ. Sci. Technol.*, 1994, **28,** 1164–1171.
418 32 J. Y. Chen, C. H. Ko, S. Bhattacharjee and M. Elimelech, Role of spatial distribution of
419 porous medium surface charge heterogeneity in colloid transport. *Colloids Surf., A*, 2001, **191,**
420 3–15.
421 33 D. L. Suarez, J. D. Rhoades, R. Lavado, and C. M. Grieve, Effect of pH on saturated
422 hydraulic conductivity and soil dispersion, *Soil Sci. Soc. AM. J.*,1984 .**48,** 50–55.
423 34 S. Lin, Y. Cheng, Y. Bobcombe, K. L. Jones, J. Liu and M. R. Wiesner, Deposition of silver
424 nanoparticles in geochemically heterogeneous porous media: Predicting affinity from surface
425 composition analysis, *Environ. Sci. Technol.*, 2011, **45,** 5209–5215.
426 35 Y. Tian, B. Gao, L. Wu, R. Munoz-Carpena and Q. G. Huang, Effect of solution chemistry on
427 multi-walled carbon nanotube deposition and mobilization in clean porous media, *J. Hazard.*
428 *Mater.*, 2012, **231,** 79−87.
429 36 A. Amirbahman and T. M. Olson, Transport of humic matter-coated hematite in packed-beds.
430 *Environ. Sci. Technol.*, 1993, **27,** 2807–2813.
431 37 A. J. Pelley and N. Tufenkji, Effect of particle size and natural organic matter on the
432 migration of nano- and microscale latex particles in saturated porous media. *J. Colloid and*
433 *Interface Sci.*, 2008, **321,** 74–83.

434 38 S. R. Deshiikan, E. Eschenazi and K. D. Papadopoulos, Transport of colloids through porous
435 beds in the presence of natural organic matter. *Colloids Surf., A*, 1998, **145,** 93–100.
436 39 Y. Li, Y. Wang, K. D. Pennell and L. M. Abriola, Investigation of the transport and
437 deposition of fullerene (C_{60}) nanoparticles in quartz sands under varying flow conditions.
438 *Environ. Sci. Technol.*, 2008, **42,** 7174–7180.
439 40 W. P. Johnson and M. Tong, Observed and simulated fluid drag effects on colloid deposition
440 in the presence of an energy barrier in an impinging jet system. *Environ. Sci. Technol.*, 2006,
441 **40,** 5015–5021.
442 41 C. Shen, Y. Huang, B. Li and Y. Jin, Predicting attachment efficiency of colloid deposition
443 under unfavorable attachment conditions. *Water Resour. Res.*, 2010, **46,** W11526.
444 42 W. P. Johnson, X. Li and G. Yal, Colloid retention in porous media: Mechanistic
445 confirmation of wedging and retention in zones of flow stagnation. *Environ. Sci. Technol.*,
446 2007, **41,** 1279–1287.
447 43 F. Wang, J. J. H. Haftka, T. L. Sinnige, J. L. M. Hermens and W. Chen, Adsorption of polar,
448 nonpolar, and substituted aromatics to colloidal graphene oxide nanoparticles, *Environ.*
449 *Pollut.*, 2014, **186,** 226–233.
450 44 Y, Gao, Y. Li, L. Zhang, H, Huang, J. Hu, S. M. Shah and X. Su, Adsorption and removal of
451 tetracycline antibiotics from aqueous solution by graphene oxides, *J. Colloid Interface Sci.*,
452 2012, **368,** 540–546.
453 45 Z. Pei, L. Li, L. Sun, S. Zhang, X. Shan, S. Yang and B. Wen, Adsorption characteristics of
454 1,2,4-trichlorobenzene, 2,4,6-trichlorophenol, 2-naphthol and naphthalene on graphene and
455 graphene oxide. *Carbon*, 2013, **51,** 156–163.

456 46 S. Pavagadhi, A. L. Tang, M. Sathishkumar, K. P. Loh and R. Balasubramanian, Removal of
457 microcystin-LR and microcystin-RR by graphene oxide: adsorption and kinetic experiments.
458 *Water Res.*, 2013, **47,** 4621–4629.

Table 1 Experimental Protocols of Column Tests.

Column No.	Column properties					Influent properties	
	Porous medium	Length (cm)	Bulk density (g/cm^3)	Porosity (-)	Pore-water velocity (m/d)	Background solution	GONPs conc. (mg/L)
1	Lula soil	7.2	1.43	0.46	10	DI water → 10 mM NaCl → 25 mM NaCl → 35 mM NaCl → 50 mM NaCl	21.1
2	Sigma sand	6.9	1.50	0.43	10	DI water → 10 mM NaCl → 25 mM NaCl → 35 mM NaCl → 50 mM NaCl	20.8
3	Lula soil	7.1	1.43	0.46	10	1.5 mM NaCl → 0.5 mM $CaCl_2$	20.6
4	Lula soil	6.8	1.42	0.46	10	0.1 mM $CaCl_2$ → 0.3 mM $CaCl_2$ → 0.5 mM $CaCl_2$	20.2
5	Sigma sand	7.1	1.58	0.41	10	1.5 mM NaCl → 0.5 mM $CaCl_2$	20.3
6	Lula soil	6.9	1.50	0.43	10	10 mM NaCl (pH 4.0)	19.5
7	Lula soil	7.0	1.44	0.46	10	10 mM NaCl (pH 7.0)	19.6
8	Lula soil	7.2	1.53	0.42	10	10 mM NaCl (pH 9.0)	19.5
9	Sigma sand	6.9	1.53	0.42	10	10 mM NaCl (pH 4.0)	20.5
10	Sigma sand	7.1	1.55	0.41	10	10 mM NaCl (pH 7.0)	19.9
11	Sigma sand	7.2	1.51	0.43	10	10 mM NaCl (pH 9.0)	19.4
12	Lula soil	6.5	1.52	0.43	10	10 mM NaCl → 10 mM NaCl + 10 mg/L SRHA	20.5
13	Lula soil	7.1	1.41	0.47	10	35 mM NaCl → 35 mM NaCl + 10 mg/L SRHA	19.9
14	Sigma sand	6.9	1.57	0.41	10	10 mM NaCl → 10 mM NaCl + 10 mg/L SRHA	21.4
15	Sigma sand	7.1	1.54	0.42	10	35 mM NaCl → 35 mM NaCl + 10 mg/L SRHA	19.7
16	Lula soil	7.1	1.45	0.45	10 → 5 → 1	10 mM NaCl	20.4
17	Sigma sand	6.9	1.58	0.40	10 → 5 → 1	10 mM NaCl	19.6

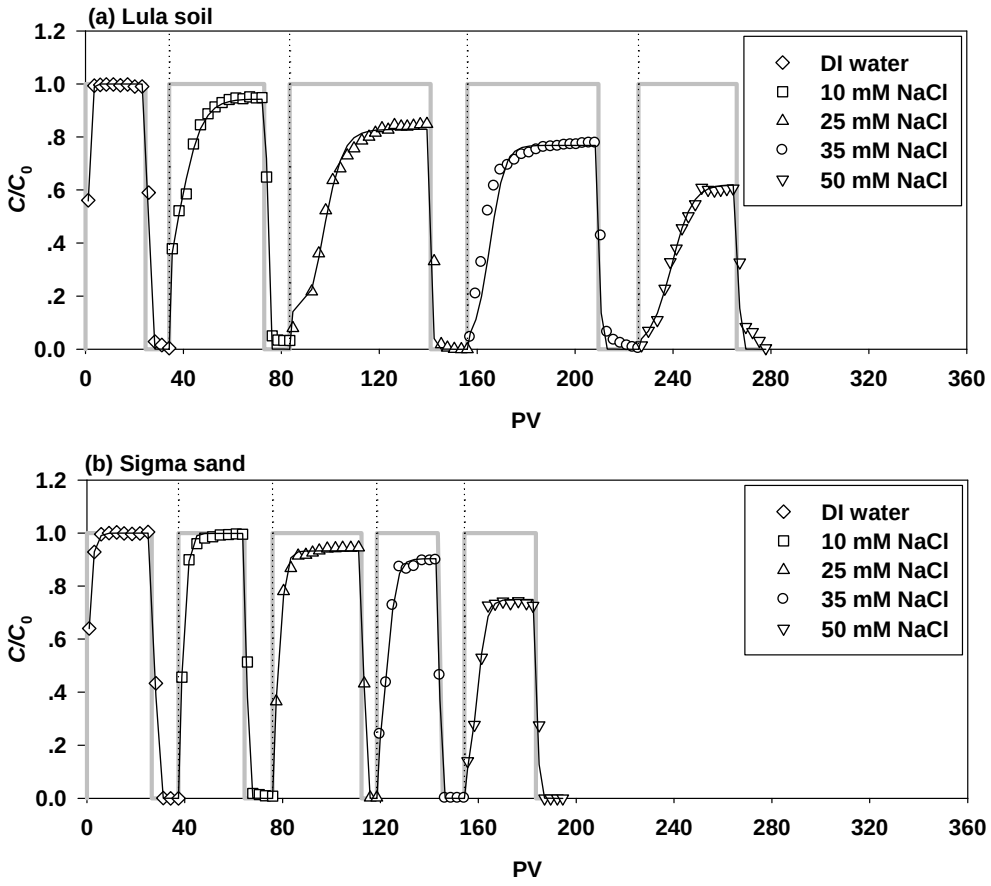

Fig. 1 Effects of ionic strength on transport of GONPs in: (a) Lula soil (Column 1); and (b) Sigma sand (Column 2). Vertical dotted lines indicate where ionic strengths were changed. Solid lines (—) was plotted by fitting the BTCs with the two-site transport model (Equations 1–5). The thick gray lines show the injected concentration of GONPs.

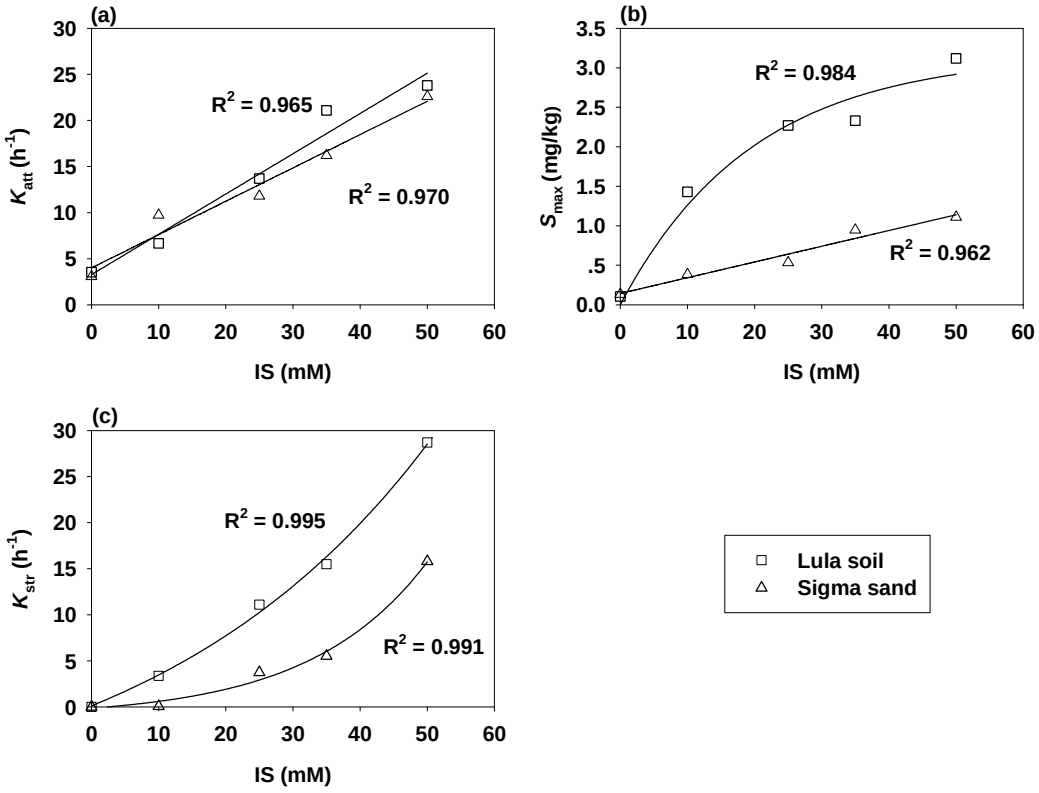

Fig. 2 Correlations between fitted parameters of two-site transport model (based on breakthrough data of Columns 1 and 2) and ionic strength.

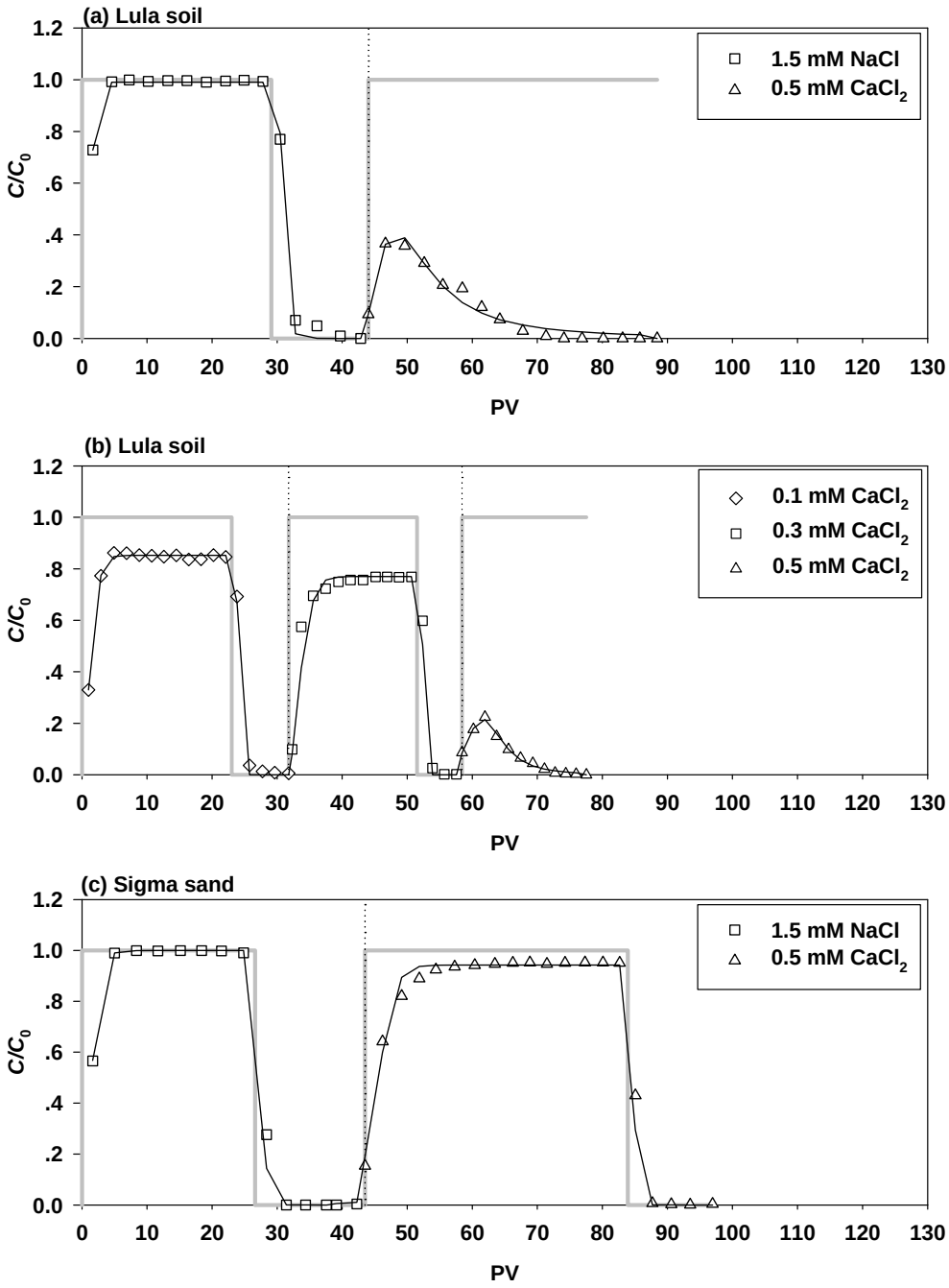

Fig. 3 Effect of Ca^{2+} on transport of GONPs in: (a) Lula soil (Column 3); (b) Lula soil (Column 4); and (c) Sigma sand (Column 5). Vertical dotted lines indicate where cationic species/concentrations were changed. Solid lines (—) was plotted by fitting the BTCs with the two-site transport model (Equations 1–6). The thick gray lines show the injected concentration of GONPs.

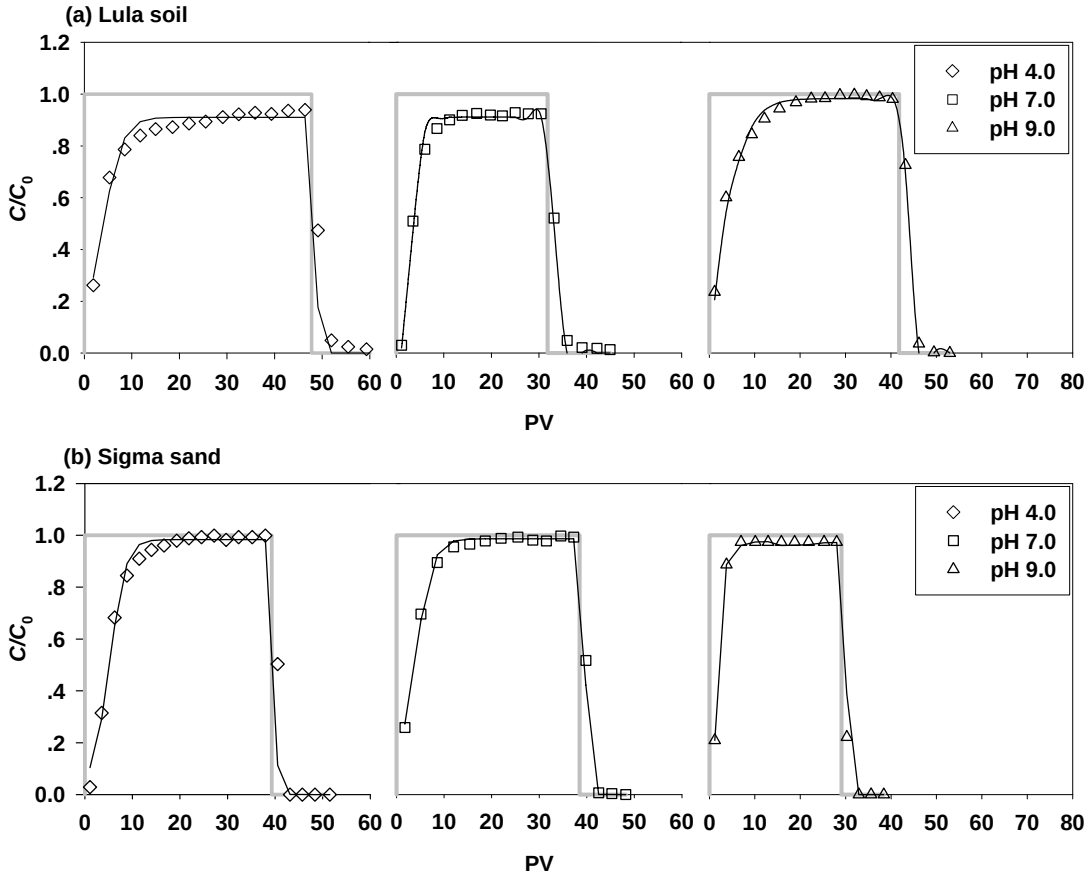

Fig. 4 Effects of pH on transport of GONPs in: (a) Lula soil (Columns 6–8); and (b) Sigma sand (Columns 9–11). Solid lines (—) was plotted by fitting the BTCs with the two-site transport model (Equations 1–5). The thick gray lines show the injected concentration of GONPs.

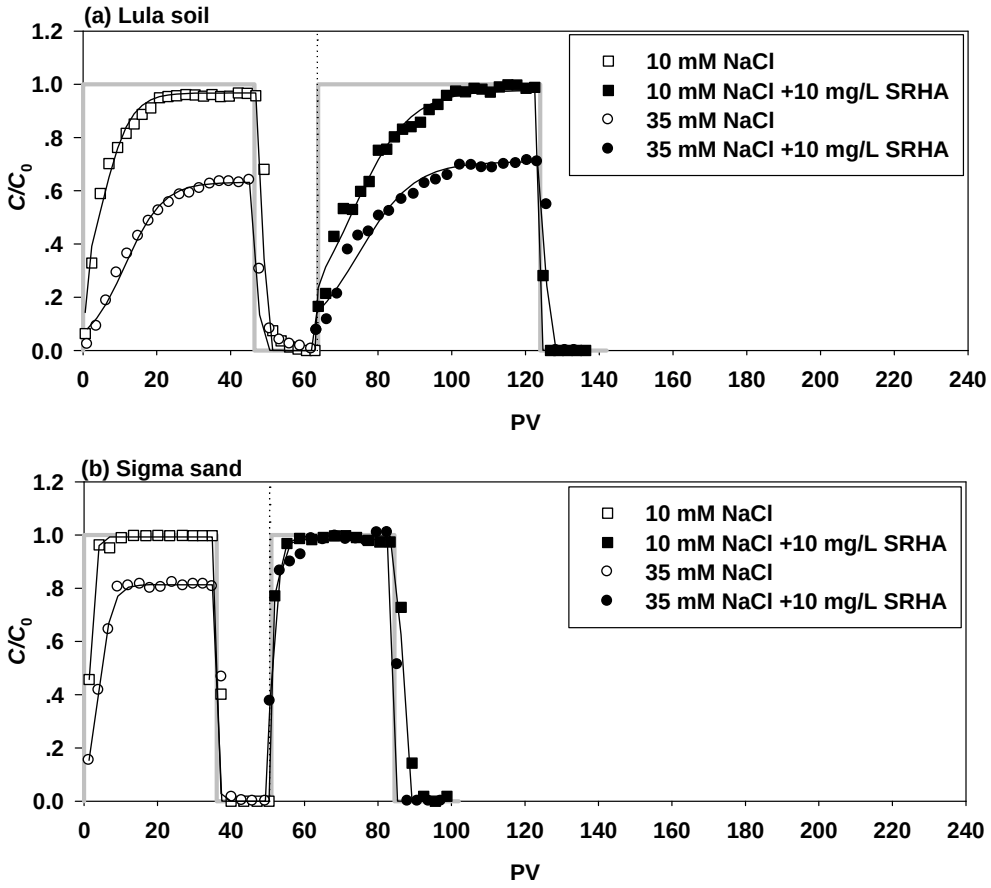

Fig. 5 Effects of Suwannee River humic acid (SRHA) on transport of GONPs in: (a) Lula soil (Columns 12 and 13); and (b) Sigma sand (Columns 14 and 15). Vertical dotted lines indicate where background electrolyte (with or without SRHA) were changed. Solid lines (—) was plotted by fitting the BTCs with the two-site transport model (Equations 1–5). The thick gray lines show the injected concentration of GONPs.

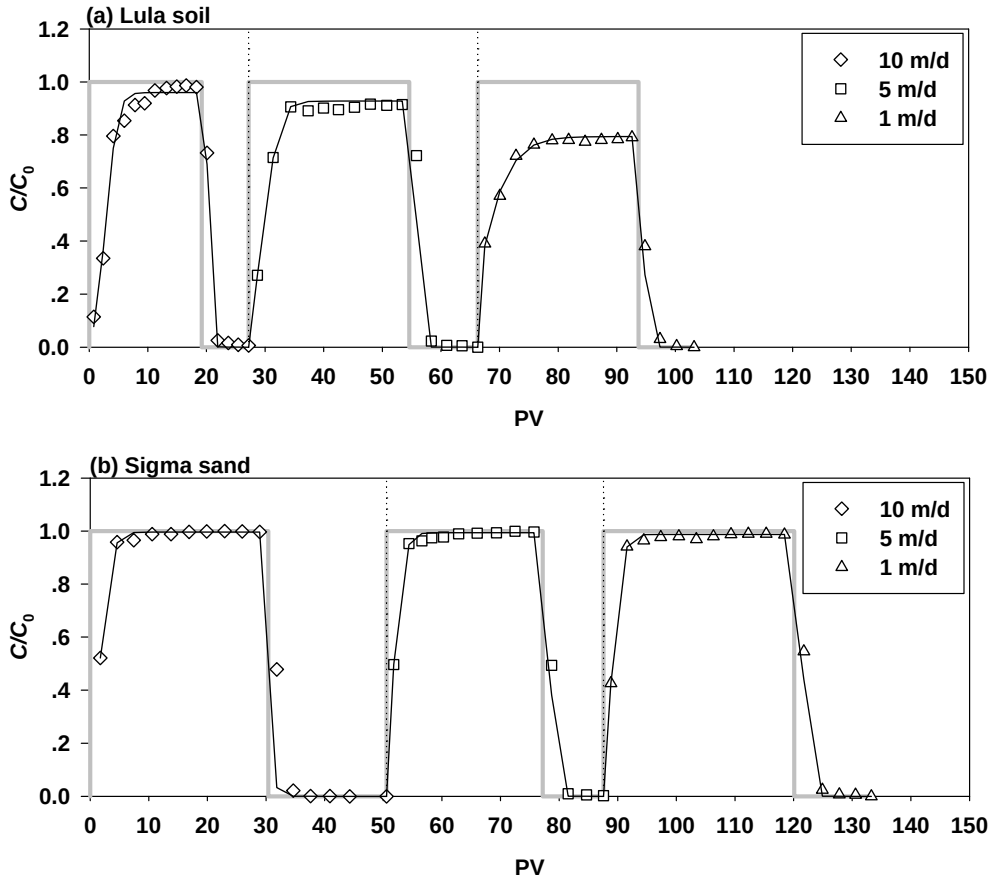

Fig. 6 Effects of flow velocity on transport of GONPs in: (a) Lula soil (Column 16); and (b) Sigma sand (Column 17). Vertical dotted lines indicate where flow velocities were changed. Solid lines (—) was plotted by fitting the BTCs with the two-site transport model (Equations 1–5). The thick gray lines show the injected concentration of GONPs.